Acta Crystallographica Section B
Structural Science
ISSN 0108-7681

Hexagonal ferrites: a unified model of the $(TS)_nT$ series in superspace

Ivan Orlov,* Lukáš Palatinus,‡ Alla Arakcheeva and Gervais Chapuis

Ecole Polytechnique Fédérale de Lausanne, Laboratoire de cristallographie, Cubotron, CH-1015 Lausanne, Switzerland

‡ Permanent address: Institute of Physics, Academy of Science of the Czech Republic, Na Slovance 2, 182 21 Prague, Czechia.

Correspondence e-mail: ivan.orlov@epfl.ch

Received 18 April 2007
Accepted 2 August 2007

Hexagonal ferrites represent an extensive family of mixed-layer magnetic materials with periods up to 1500 Å along the stacking direction, probably constituting the largest unit cells in the inorganic realm. The $(TS)_nT$ subfamily includes $P\bar{3}m1$ and $R\bar{3}m$ structures that can be derived from Y ferrite $Ba_2M_2Fe_{12}O_{22}$ (M = Zn, Fe, Co, Mg, Mn) by introducing stacking faults. A unified $(3+1)$-dimensional superspace model is proposed for all members of the $(TS)_nT$ family. The model belongs to the superspace group $X\bar{3}m1(00\gamma)$ with $X = \{(\frac{1}{3}, \frac{2}{3}, 0, \frac{1}{3}), (\frac{2}{3}, \frac{1}{3}, 0, \frac{2}{3})\}$, has a unit cell of the basic structure with a = 5.88, c = 4.84 Å and modulation vector $\mathbf{q} = \frac{4n+3}{9n+6}\mathbf{c}^*$, where n is rational for periodic structures and irrational for the aperiodic ones. The model was tested on calculated data of one of the principal members of the $(TS)_nT$ family, the Y ferrite ($n = \infty$). The fit obtained with the superspace model was excellent. The model allowed a reduction of refinable parameters by 19% with respect to the ordinary refinement without a significant increase of the refinement R values.

1. Introduction

The superspace concept is a crystallographic approach for the generalization of symmetry, structural models and structure-dependent properties (van Smaalen, 2007; Janssen *et al.*, 2007). Although the original motivation for the development of the superspace formalism was the description of aperiodic crystals, the concept gained general acceptance in a wider range of applications. In particular, the method is able to combine related structures into a single model, thus offering a clearer view of their hidden relationships. While the individual members of the family can have different space-group symmetries and be either periodic or aperiodic, the generalization in superspace leads to a common crystallographic structure model and a common superspace group uniting all of them (Pérez-Mato *et al.*, 1999). The benefits of such a model are best demonstrated if applied to an extensive and diverse family of compounds.

Hexagonal ferrites represent a prominent example of such an extensive family and are widely known for their applications in motors, consumer electronics, microwave technology and, recently, in medicine. Currently the family includes more than 60 members of magnetic materials with unit-cell dimensions extending up to 1577 Å (Kohn *et al.*, 1971). The study of compounds approaching such a protein-like magnitude is necessarily complicated by different symmetries of individual structures and by the large number of possible structure models, generated by different stacking of several building units. Fortunately, the generalization in higher dimensional

space offers a mechanism for solving these difficulties. The description of the family is not only more elegant but also reveals characteristic relations which are not easily observable while dealing with individual structures.

2. Hexagonal ferrites

Ferrites in general are complex oxides composed of various metals and oxygen. By varying the metal atoms in the structure, one can produce virtually an infinite number of compounds with various magnetic properties. In magnetic oxides, the O atoms form an essentially fixed skeleton that can be filled in a number of different ways by various metals. 'Hexagonal ferrites', named in opposition to cubic or spinel ferrites, form a particular group closely related to the mineral *magnetoplumbite* with the approximate chemical composition $Pb[Fe,Mn]_{12}O_{19}$. Five principal members termed *M*, *W*, *Z*, *X* and *Y* were extensively described by Braun (1957). Fig. 1 shows the chemical compositions of the compounds in the ternary phase diagram for the BaO–*M*O–Fe_2O_3 system. A more detailed diagram for the *M* = Ti system was recently reported by Siegrist & Vanderah (2003).

The $(TS)_nT$ subfamily discussed below was initially discovered by Kohn & Eckart (1963) and is closely related to the Y ferrite with chemical composition $Ba_2M_2Fe_{12}O_{22}$ (*M* = Zn, Fe, Co, Mg, Mn) and space group $R\bar{3}m$. Its unit cell with $c = 43.56$ Å includes 18 oxygen layers (Fig. 2*a*). The cell can be divided into three parts symmetrically related by the *R* centering. Each part contains four successive oxygen layers followed by two layers with one quarter of O atoms replaced by barium.

For the purpose of the present analysis we split the sequence into two stacking units called S and T (Braun, 1957), which are structurally related to the parent structure of cubic spinel *M*O–Fe_2O_3. The S block is a two-layers thick (111) slice of the cubic spinel structure. Two tetrahedral interstices and four octahedral interstices between the oxygen layers are occupied by the metal atoms. The T block consists of four oxygen layers. In the two interior layers one fourth of the O atoms are replaced by barium. Small cations are distributed among five interstices, two tetrahedral and three octahedral (Fig. 3). Cations at the octahedral sites lie on a threefold axis, and their coordination octahedron shares faces with two adjacent empty octahedra. The chemical composition and

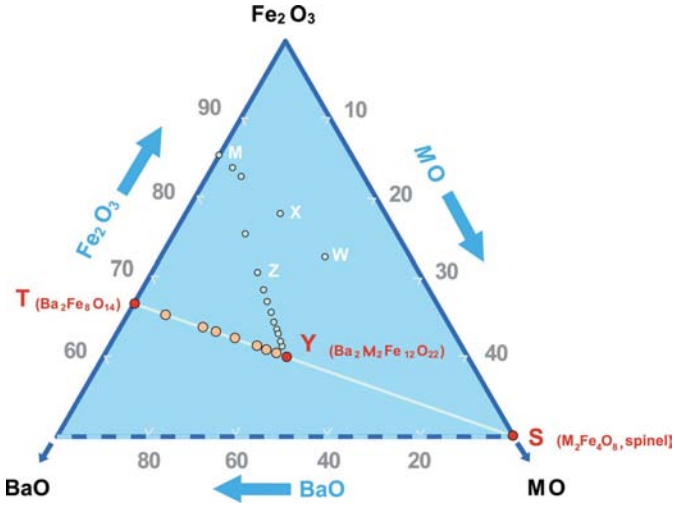

Figure 1
Composition diagram for hexagonal ferrites. The connecting line between T and S indicates the $(TS)_nT$ family stoichiometry.

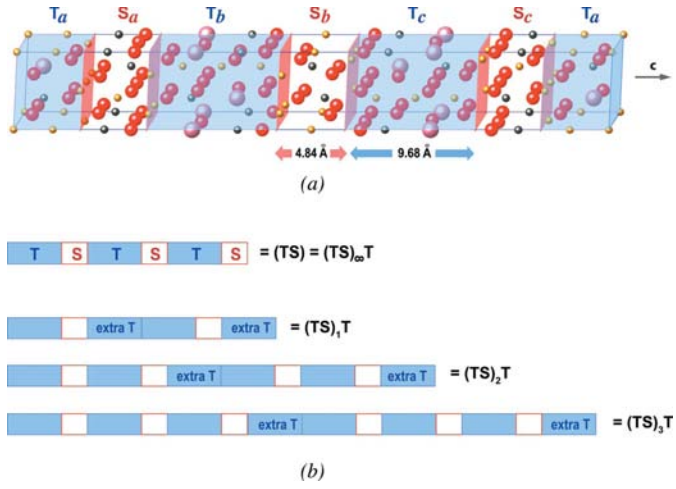

Figure 2
(*a*) S and T building blocks and the stacking sequence of Y ferrite, $Ba_2M_2Fe_{12}O_{22}$ (space group $R\bar{3}m$, $a = 5.88$, $c = 43.6$ Å; Braun, 1957). Ba atoms are pink, O atoms red, Fe atoms yellow, *M* (Zn, Co, Ti) black. To visualize the layers better, some extra atoms located outside of the unit cell are depicted. (*b*) Schematic representation of the block sequences used in the modelling of the $(TS)_nT$ series. Sequences correspond to $n = \infty$ [parental Y ferrite, see (*a*)] and n = 1, 2, 3. Indices of blocks indicating their *x* and *y* positions (see text) are omitted for simplicity. Extra T blocks are considered as stacking faults.

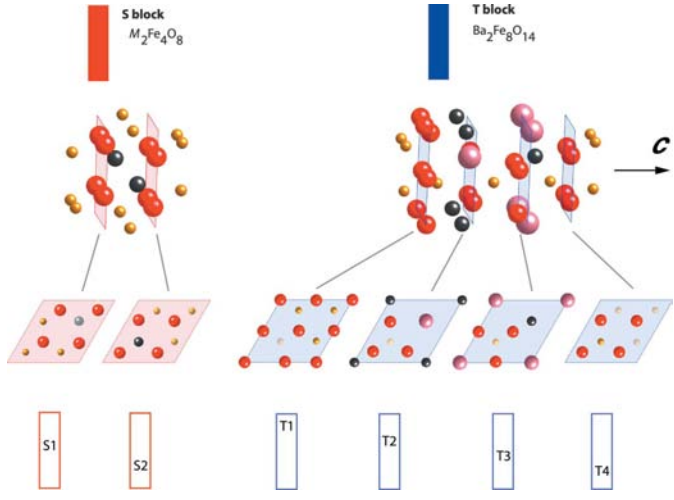

Figure 3
S and T building blocks: individual oxygen layers and the corresponding occupation domains. Ba atoms are pink, O atoms red, Fe atoms yellow, *M* (Zn, Co, Ti) black. Blue and red bars for T and S occupation domains correspond to Fig. 6. Generally the exact location of the atoms within S and T blocks depends on the *xy* position of the block. Blocks shown here correspond to S_b and T_c blocks in Fig. 2.

Table 1
Chemical and crystallographic data for members of the $(TS)_nT$ structural series (Kohn & Eckart, 1963; Kohn *et al.*, 1971; Pollert, 1985).

The structure of T ferrite ($n = 0$) is only hypothetical.

n	Stacking sequence	Space group	Layers in unit cell	Composition	c parameter (Å)
0	$(TS)_0T = (T)_3$	$P\bar{3}m1$	$4 \times 3 = 12$	$Ba_2Fe_8O_{14}$	29.07
1	$(TS)_1T$	$R\bar{3}m$	30	$Ba_4Zn_2Fe_{20}O_{36}$	72.6
2	$(TS)_2T$	$R\bar{3}m$	48	$Ba_6Zn_4Fe_{32}O_{58}$	116.2
3	$(TS)_3T$	$P\bar{3}m1$	$22 \times 3 = 66$	$Ba_8Zn_6Fe_{44}O_{80}$	159.7
4	$(TS)_4T$	$R\bar{3}m$	84	$Ba_{10}Zn_8Fe_{56}O_{102}$	203.0
5	$(TS)_5T$	$R\bar{3}m$	102	$Ba_{12}Zn_{10}Fe_{68}O_{124}$	247.0
6	$(TS)_6T$	$P\bar{3}m1$	$40 \times 3 = 120$	$Ba_{14}Zn_{12}Fe_{80}O_{146}$	290.4
7	$(TS)_7T$	$R\bar{3}m$	138	$Ba_{16}Zn_{14}Fe_{92}O_{168}$	334.0
8	$(TS)_8T$	$R\bar{3}m$	156	$Ba_{18}Zn_{16}Fe_{104}O_{190}$	378.0
∞	$(TS)_\infty T = (TS)_3$	$R\bar{3}m$	18	$Ba_2Zn_2Fe_{12}O_{22}$ (Y ferrite)	43.6

internal organization of S and T blocks do not depend on the stoichiometry of a particular compound, therefore we consider them as rigid stacking units.

The *Y* structure can be constructed by alternate stacking of the T and S units along the (001) direction. Every TS pair of blocks is shifted with respect to the previous TS pair by $(\frac{1}{3},\frac{2}{3})$ in the **ab** plane. To distinguish the different positions of the blocks we shall use subscript indices *a*, *b* and *c* in order to indicate the number of applied shifts (0, 1 and 2, respectively). The crystallographic build-up of the *Y* structure is thus represented by the $T_aS_aT_bS_bT_cS_c$ sequence or shortly $(TS)_3$.

The derived structures involve extra T blocks on a periodic basis. Starting with an ideal (TS) stacking along the (001) direction, the extra T blocks can be seen as a result of a stacking fault between two successive TS units. These TT faults occur in the $T_aS_aT_bS_bT_cS_c$ reference sequence when one of the T blocks is not directly followed by an S block, but by an identical T block which is then followed by the 'expected' S block (Fig. 2*b*).

Electron microscopy and direct lattice imaging of known periodic ferrites show that these faults are distributed along the stacking sequence in the most uniform way, forming a *uniform sequence* (Kohn & Eckart, 1963; Van Landuyt *et al.*, 1973; Pollert, 1985). If we assume that this principle of uniform distribution is of general validity for any composition, then the actual layer sequence for a given composition parameter n is always given by the $(TS)_nT$ formula. The range of compositions covered by various values of n lies on the line connecting T and S on the compositional diagram (Fig. 1), and is limited by the Y ferrite ($n = \infty$) and the hypothetical T ferrite ($n = 0$).

Let us investigate the periodicity of a $(TS)_nT$ structure along the stacking direction. Since each consecutive TS pair in the regular sequence is shifted by $(\frac{1}{3},\frac{2}{3})$ in the **ab** plane, it follows that every extra T block will occur at the position $(\frac{n \bmod 3}{3},\frac{2n \bmod 3}{3})$ from the origin. The structure will have the stacking periodicity corresponding to the distance of two TT faults with the same in-plane shift. In the case of commensurate structures this leads to two distinct cases with different symmetries: $n \neq 3k$ and $n = 3k$, $k \in \mathbb{N}_0$.

2.1. $n \neq 3k$

In this case three TT faults are necessary to form a unit cell. Hence the translation vector between consecutive TT faults is $(\frac{1}{3},\frac{2}{3},\frac{1}{3})$, which corresponds to the reverse *R* centering, or $(\frac{2}{3},\frac{1}{3},\frac{1}{3})$ for the obverse *R* centering. The resulting unit cell will have the space group $R\bar{3}m$. These structures can be denoted as $[(TS)_nT]_3$, where the subscript '3' denotes the tripling of the basic $(TS)_nT$ sequence.

As an example, the structure with $n = 1$ contains one TT fault after every TS double block. The corresponding sequence is $T_aS_aT_bT_bS_bT_cT_cS_cT_a$. The sequence for $n = 2$ is analogously

$$T_aS_aT_bS_bT_cT_cS_cT_aS_aT_bT_bS_bT_cS_cT_a = [(TS)_2T]_3.$$

The *Y* ($n = \infty$) structure also has the symmetry $R\bar{3}m$ and can thus be formally included in the $n \neq 3k$ class.

2.2. $n = 3k$

In this case the consecutive TT faults have the same position in the **ab** plane and the periodicity is given by only one $(TS)_nT$ sequence. Thus, the cell is not *R* centered and the periodicity is only one third of the periodicity of the $n \neq 3k$ case; the space group becomes $P\bar{3}m1$. However, to treat all possible structures on the same basis, we will consider the unit-cell dimension of the $n = 3k$ case to be the same as of the $n \neq 3k$ case, *i.e.* the distance of three TT faults.

The simplest example of a $n = 3k$ sequence is the case $n = 3$

$$T_aS_aT_bS_bT_cS_cT_aT_aS_aT_bS_bT_cS_cT_aT_aS_aT_bS_bT_cS_cT_a = (TS)_3T.$$

Members of the $(TS)_nT$ series are listed in Table 1, including the border cases $n = 0$ (hypothetical T phase) and $n = \infty$ (the *Y* ferrite). However, it is reasonable to expect the existence of other structures with various n, which are not mentioned here. This especially concerns the incommensurately modulated structures where n is a non-integer.

3. Unit cell and modulation wavevector

By taking n as a composition-dependent parameter, the members of the $(TS)_nT$ series can be described by the formula $Ba_{2n+2}M_{2n}Fe_{12n+8}O_{22n+14}$. The *a* unit-cell parameter approximately equals 5.88 Å for every member. The number of T and S blocks in the unit cell defines the *c* parameter. There are $3n + 3$ T blocks with four oxygen layers, and $3n$ S blocks with two oxygen layers in a $[(TS)_n]_3$ sequence. This yields $18n + 12$ oxygen layers per unit cell. The average layer-to-layer distance is approximately 2.42 Å (Braun, 1957), yielding $c \simeq 2.42\,(18n + 12)$ Å. In the construction of the ideal model we shall assume that the location of 'small' atoms, such as Fe and Zn, is strictly defined by the encompassing oxygen layers.

For the superspace embedding, a structural model needs to be defined for which the description of any member of the family is reduced to an occupation modulation of a unique basic structure. There are several possibilities for selecting the unit cell of the basic structure. However, because the S block represents the smallest rigid unit and it has two oxygen layers, it is a natural choice to select the period of two oxygen layers as the c parameter of the unit cell of the basic structure (*basic unit cell* in short). Since the length of the $[(TS)_nT]_3$ sequence is $18n + 12$ oxygen layers, it follows that the modulation vector must be of the form $(0, 0, \gamma)$ with $\gamma = \frac{2k}{18n+12}$, where k and $18n + 12$ do not have any common divisor. This relation establishes a direct link between the composition and the modulation vector. A suitable value of k can be determined from diffraction patterns and will be defined in §4.

4. Diffraction patterns

While the structures of the few principal ferrites are well described and the corresponding structural data are easily available (Braun, 1957; Soohoo, 1960), obtaining the atomic positions for intermediate family members is more difficult. In former publications, only the stoichiometry is given, while structural data are absent or deficient (Kohn & Eckart, 1963, 1965). Therefore, we simulated the electron diffraction patterns (EDP) of several phases from the atomic arrangements of the T and S blocks and from the sequence of the blocks. As a source of the atomic coordinates of the T and S blocks we used the structure of the Y ferrite determined by Shin & Kwon (1993). The EDPs were simulated with the *SingleCrystal* software (CrystalMaker Software Ltd, 2007) for a wavelength of 0.037 Å and a sample thickness of 30 Å.

The (00l) rows of the patterns (Fig. 4) exhibit spots with a clear dependence on the composition parameter n. The position of the spots indexed as 0 0 6 for n = 0, 0 0 15 for n = 1, 00 24 for n = 2 and their analogues for other compositions remain unchanged from pattern to pattern. These reflections are associated with the reciprocal distance 0.207 Å^{-1}, which in real space yields 4.8 Å and corresponds to two O-atom layers or the thickness of the S block. This is exactly the c parameter of the basic unit cell chosen in the previous section. Thus, these reflections correspond to the 0 0 1 0 reflection in the (3 + 1)-dimensional indexing independently of the compound they belong to.

The spots not indexable with the reciprocal basic unit cell are composition dependent and shall be considered as satellites. They can be indexed using a vector of the general form $l\mathbf{c}^* + m\mathbf{q}$, *i.e.* (00$lm$). It has already been mentioned in the previous section that the choice of the modulation vector $\mathbf{q}$ in the set of purely commensurate structures is not unique. However, there is usually a choice that is more convenient for practical reasons. In our case, there are spots which are always strong and whose location varies smoothly with composition. We decided to consider the vector from the origin to these satellite peaks as the composition-dependent $\mathbf{q}$ vector. However, as a result of the non-standard centering of the (3 + 1)-dimensional unit cell along $\mathbf{a}_{s4}$ (see §5) the diffraction pattern fulfills the reflection condition $m = 3n$ for the 00lm reflections. Noting that the reflections 0001 and 0002 are absent, we conclude that the strong spots will have indices 0003. The corresponding modulation vector is indicated by red arrows in Fig. 4. The modulation vector has the form $(0, 0, \gamma)$, and for n = 0, 1 and 2 this scheme yields the values $\gamma = \frac{1}{2}, \frac{7}{15}$ and $\frac{11}{24}$, respectively. The γ component of the modulation vector can be generally expressed as $\gamma = \frac{4n+3}{9n+6} = \frac{8n+6}{18n+12}$. The latter fraction underlines the relation between the modulation vector and the total number of oxygen layers in the three-dimensional unit cell. The selected modulation vector allows any satellite spot to be indexed. The principle used to

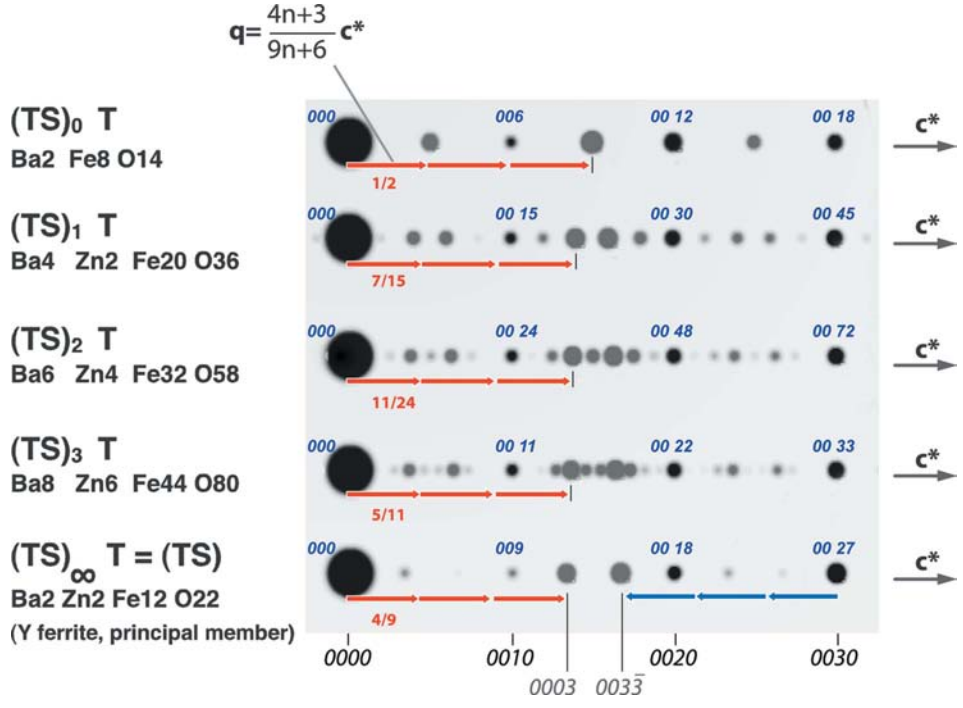

Figure 4
The three-dimensional (small) and (3 + 1)-dimensional indexing of 00l reflections observed in electron diffraction patterns (EDP) for n = 0, 1, 2, 3 and ∞. The patterns are simulated based on Kohn & Eckart (1963), Pollert (1985) and Shin & Kwon (1993). Using c = 4.84 Å (two oxygen layers) and $\mathbf{q} = \frac{4n+3}{9n+6}\mathbf{c}^*$ the indexing with four indices (00lm) is uniform for all the patterns. The modulation vectors are shown by arrows. The reflection condition $m = 3n$ (see §5) is observable in the patterns. As an example, another line of modulation vectors is shown starting from the reflection 0030 to illustrate that indexing of other spots is possible.

Table 2
Symmetry operations of the superspace group $X\bar{3}m1(00\gamma)$ with $X = \{(\frac{1}{3}, \frac{2}{3}, 0, \frac{1}{3}),(\frac{2}{3}, \frac{1}{3}, 0, \frac{2}{3})\}$ and the resulting reflection condition.

Generators of the superspace group $X\bar{3}m1(00\gamma)$	
$t\ (\frac{1}{3}, \frac{2}{3}, 0, \frac{1}{3})$	$(x1 + \frac{1}{3}, x2 + \frac{2}{3}, x3, x4 + \frac{1}{3})$
$3_{0,0,z}$	$(-x2, x1 - x2, x3, x4)$
$\bar{1}$	$(-x1, -x2, -x3, -x4)$
$2_{x,x,0}$	$(x2, x1, -x3, -x4)$
Reflection conditions	
$hklm$	$h - k + m = 3n$

Table 3
Space groups for commensurate structures with superspace group $X\bar{3}m1(00\gamma)$ with $X = \{(\frac{1}{3}, \frac{2}{3}, 0, \frac{1}{3}),(\frac{2}{3}, \frac{1}{3}, 0, \frac{2}{3})\}$ depending on the parity of the numerator s and denominator r of $\gamma = \frac{s}{r}$; k and m are arbitrary integers.

$\gamma = \frac{s}{r}$	$\frac{3k}{3m+1}$	$\frac{3k}{3m-1}$	$\frac{3k\pm1}{m}$
$t_0 = \frac{k}{2r}$	$R\bar{3}m_{\rm obverse}$	$R\bar{3}m_{\rm reverse}$	$P\bar{3}m1$
$t_0 =$ arbitrary	$R3m_{\rm obverse}$	$R3m_{\rm reverse}$	$P3m1$

index the diffraction pattern with four indices is schematized in Fig. 5.

5. Superspace group

The superspace group for the $(TS)_n$T subfamily should generate the space groups $R\bar{3}m_{\rm obverse}$, $R\bar{3}m_{\rm reverse}$ and $P\bar{3}m1$ for rational values of γ. The database relating three-dimensional and (3 + 1)-dimensional symmetry, *Superspace Finder* (Orlov & Chapuis, 2004–2007), yields the superspace group $R\bar{3}m(00\gamma)$ as the only superspace group meeting this criterion. This superspace group leads to a reflection condition $hklm$: $h - k + l = 3n$, and as a result the first observed main reflection in the 00lm rows shown in Fig. 4 would have the index 0030. This corresponds to a tripled value of the c parameter of the basic unit cell. We prefer to operate with the c parameter equal to two oxygen layers, as was elucidated in §3. Therefore, we transform the standard setting $R\bar{3}m(00\gamma)$ to an equivalent setting $X\bar{3}m1(00\gamma)$ with the non-standard centering X given by the generating vector $(\frac{1}{3}, \frac{2}{3}, 0, \frac{1}{3})$ leading to the reflection condition $h - k + m = 3n$. In this setting both the c parameter and the modulation vector are reduced to one third with respect to the standard setting. It is this setting of the superspace group that is used throughout this work.

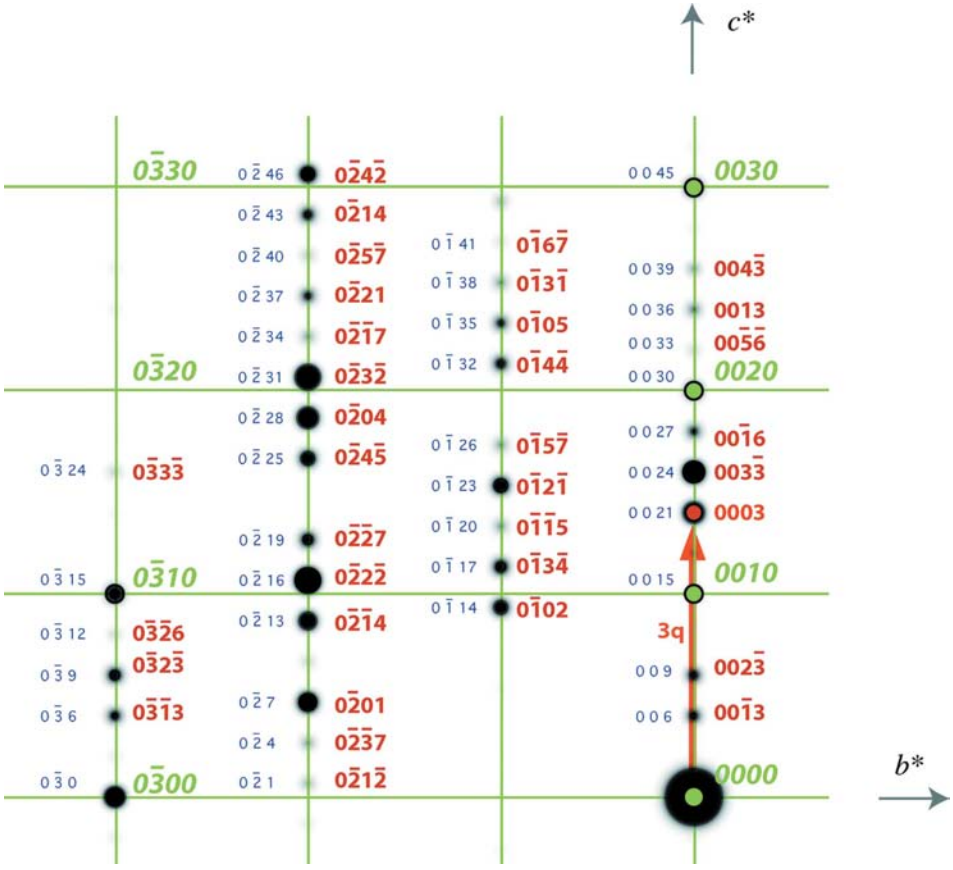

Figure 5
The three-dimensional and the (3 + 1)-dimensional indexing of the 0klm plane of a diffraction pattern for $n = 1$ ($Ba_4Zn_2Fe_{20}O_{36}$). The pattern was simulated using data from Shin & Kwon (1993). Small indices represent a three-dimensional lattice ($R\bar{3}m$, a = 5.88, c = 72.6 Å), bold italic for (3 + 1)-dimensional average lattice $hkl0$ and the roman bold for satellite reflections (modulation vector $\mathbf{q} = \frac{7}{15}\mathbf{c}^*$). The lattice of the main reflections is indicated by a grid. It can be observed on the image that the reflections follow the reflection condition $h - k + l = 3n$ for the three-dimensional indexing and $h - k + m = 3n$ for the (3 + 1)-dimensional indexing.

The list of symmetry operations for the superspace group $X\bar{3}m1(00\gamma)$ is given in Table 2. The possible three-dimensional space groups for the rational **q** vector can be obtained by applying simple algebraic rules (Tamazyan *et al.*, 1996), and are listed in Table 3, depending on γ and the starting phase t_0. It follows from the table that for a given value of γ the choice of the three-dimensional space goup is limited to only two possibilities, depending on the particular value of the starting phase t_0, *i.e.* the section in superspace which corresponds to the real space structure. To our knowledge, all the periodic $(TS)_n$T phases reported so far (Kohn & Eckart, 1963; Kohn *et al.*, 1971; Pollert, 1985) belong to the space groups listed in Table 3.

6. Construction of the superspace model

The basic characteristics of the proposed (3 + 1)-dimensional model were defined in the previous sections. The a unit-cell parameter is identical for all $(TS)_n$T structures, and it remains unchanged in the (3 + 1)-dimen-

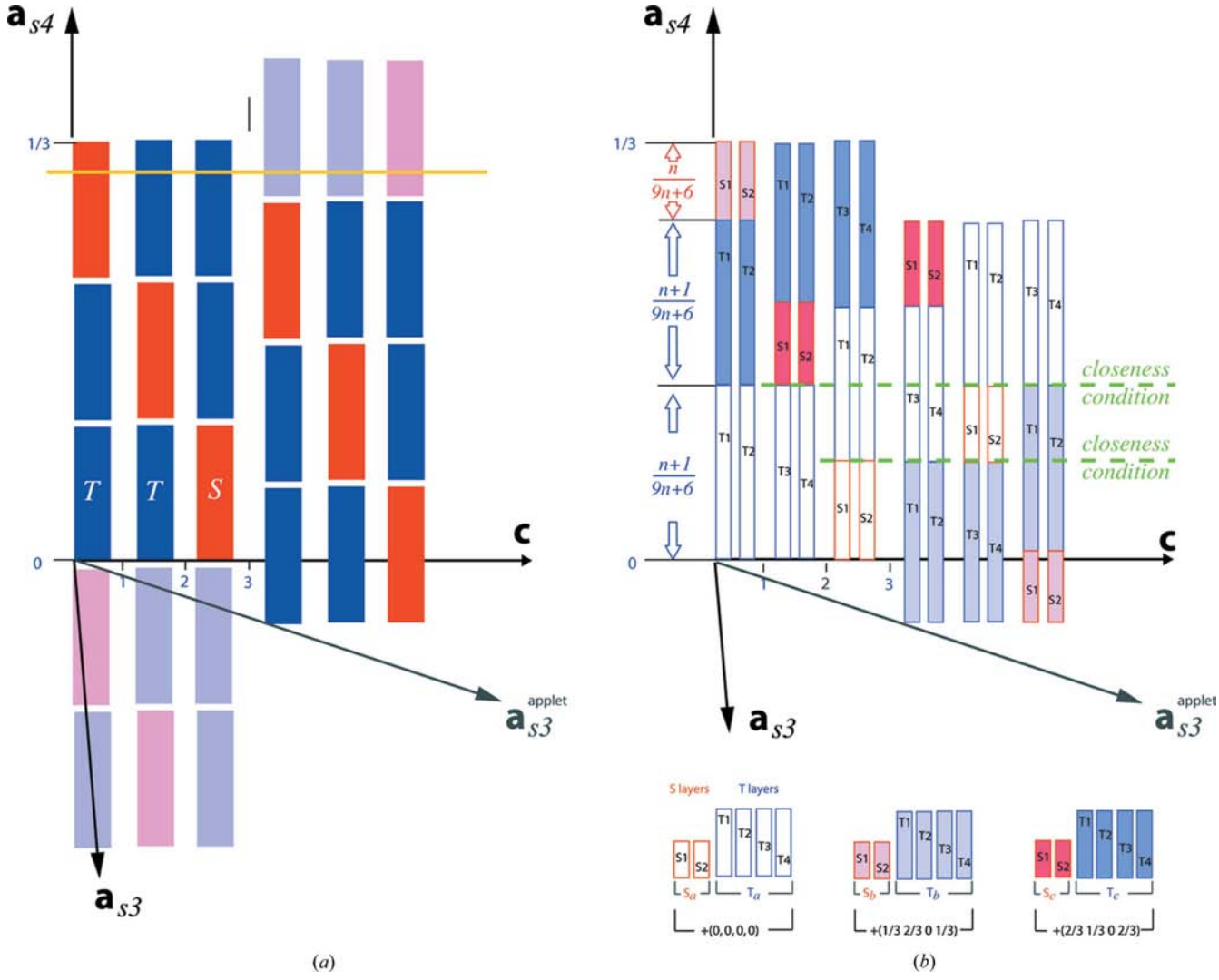

Figure 6
Assembling of the superspace model. (*a*) A preliminary model at the level of building blocks. In this model the vertical sizes of T and S occupation domains are set equal and *xy* shifts between blocks are not shown. The yellow line indicates a cut with a TT fault. Since the width of the occupation domains is not set properly, the closeness condition is not fulfilled and thus incorrect half T blocks occur. The $\mathbf{a}_{s3}^{\rm applet}$ axis corresponds to a unit cell nine times larger which is used in interactive models on http://superspace.epfl.ch/ferrites/applet2.html. The gaps between the blocks are added to the image for lucidity and are not present in the model itself. (*b*) Each block is split into atomic layers, the domain lengths along *x*4 are properly adjusted, and the corresponding *xy* shifts are indicated by color. White represents unshifted blocks, which are taken as a reference point, and more intense colors indicate blocks which underwent one or two translations. In this model the closeness condition is already met.

sional unit cell, while c = 4.84 Å and $\mathbf{q} = \frac{4n+3}{9n+6}\mathbf{c}^*$, as defined above.

Fig. 6 illustrates the assembling of the superspace model. The vertical axis $\mathbf{a}_{s4}$ represents the internal space dimension and the horizontal axis is the stacking direction **c**. The blue and red occupation domains along the internal space indicate oxygen layers belonging to T and S blocks, respectively. The S block consists of two oxygen layers while the T block includes four, *i.e.* twice that number (Fig. 3). For the initial model we assume that one occupation domain in Fig. 6(*a*) describes two consecutive oxygen layers and thus the representation of the T block requires two adjacent occupation domains – one for the layers 1 + 2 and one for the layers 3 + 4.

In real space the block sequence is obtained as a horizontal cut (**c** axis) of the construction where the z coordinate in the three-dimensional physical space is defined by the x_3 coordinate in the (3 + 1)-dimensional superspace. The occupation domains are translated along the $\mathbf{a}_{s3}$ axis due to the periodicity of the (3 + 1)-dimensional unit cell. The inclination of the $\mathbf{a}_{s3}$ axis depends on the value of $\gamma = \frac{4n+3}{9n+6}$. Consequently, for some horizontal cuts the layer sequence in real space will be modified, and, in particular, four successive T block domains, *i.e.* a TT fault, can be found in the sequence. An example of such a fault can be seen directly below the $t = \frac{1}{3}$ level (yellow horizontal line in Fig. 6*a*), where two T domains come into contact along **c**.

The ratio between the S and T blocks in a $(TS)_nT$ sequence is $\frac{n}{n+1}$. The volume occupied by the T and S occupation domains in the superspace model must consequently follow the same ratio. Since there are two T domains and one S

domain per one third of the periodicity along $\mathbf{a}_{s4}$, the T domain must have an x_4 length $L_T = \frac{n+1}{9n+6}$ and the S domain $L_S = \frac{n}{9n+6}$. With increasing n, L_T will increase slower than L_S, thus decreasing the presence of the T blocks. With these lengths of the occupation domains it will be guaranteed that an S domain will always be followed by two consecutive T domains, and thus no 'half-T blocks' can occur (compare Figs. 6*a* and *b*). This condition is equivalent to fulfilling the closeness condition (Cornier-Quiquandon *et al.*, 1992; Zakhour-Nakhl *et al.*, 2000).[1]

The construction of Fig. 6(*b*) shows T and S blocks with resolved individual oxygen layers. They are numbered according to their stacking order inside the corresponding block (Fig. 3). In real space the identical building units appear shifted by a translation of $\left(\frac{1}{3}, \frac{2}{3}\right)$ parallel to the **ab** plane (Fig. 2). In Fig. 6 this shift is illustrated by color intensity.[2]

Each occupation domain from Fig. 6 can be further split to describe individual atoms instead of the whole layers, as illustrated in Fig. 7. Atomic positions and the positions of the occupation domains of individual atoms are listed in Table 4.

The number of domains can be reduced by joining atomic occupation domains connected across the border between blocks. This involves pairs of atoms O1_T1 + O1_S1, O2_T1 + O5_S1, Zn1_T1 + Zn2_S1 and Fe4_T4 + Fe2_S2 (see Fig. 7). This joining reduces the number of atomic positions in the superspace model from 12 to 9, while leaving the resulting three-dimensional constructions intact.

The inversion centers are located in the middle and at the borders of the blocks (*cf.* Fig. 8). Since the lengths of the blocks change with n, so does the position of the inversion center. If the origin of the unit cell should coincide with the origin of the S block independently of n, the origin of the superspace group has to be shifted. We selected as a reference the inversion center with the coordinates $(0, 0, \frac{1}{4})$ (shown in bold in Fig. 8). This inversion center is located at the border of the layers T1 and T2, and thus has the t coordinate equal to $\frac{2n+1}{9n+6}$. The x_4 coordinate follows from $x_4 = t + \mathbf{qr}$, where $\mathbf{r} = \left(0, 0, \frac{1}{4}\right)$ as $\frac{12n+7}{36n+24}$. Thus, the origin shift of the superspace group from the standard setting with the inversion center in the origin becomes $\mathbf{s} = (0, 0, -\frac{1}{4}, -\frac{12n+7}{36n+24})$.

7. Refinement of the Y ferrite, $n = \infty$

The layered model presented above involves some idealizations and must be combined with the displacive modulation of the atoms to describe a real structure. For example, the Ba atoms are larger than the O atoms and they lie approximately 0.25 Å out of the plane of the oxygen to satisfy the bond-valence conditions. The distance between a layer with a barium and the following oxygen layer is reduced from 2.42 to 2.35 Å.

These deviations from the ideal model can be incorporated in the superspace model as deviations of the basic positions of the atoms from their ideal positions as well as changes of the shape of the modulation functions from a constant function to a more general shape.

To demonstrate that the general model is also able to describe a real structure and to validate the model we decided to refine the model against the real data of a ferrite structure.

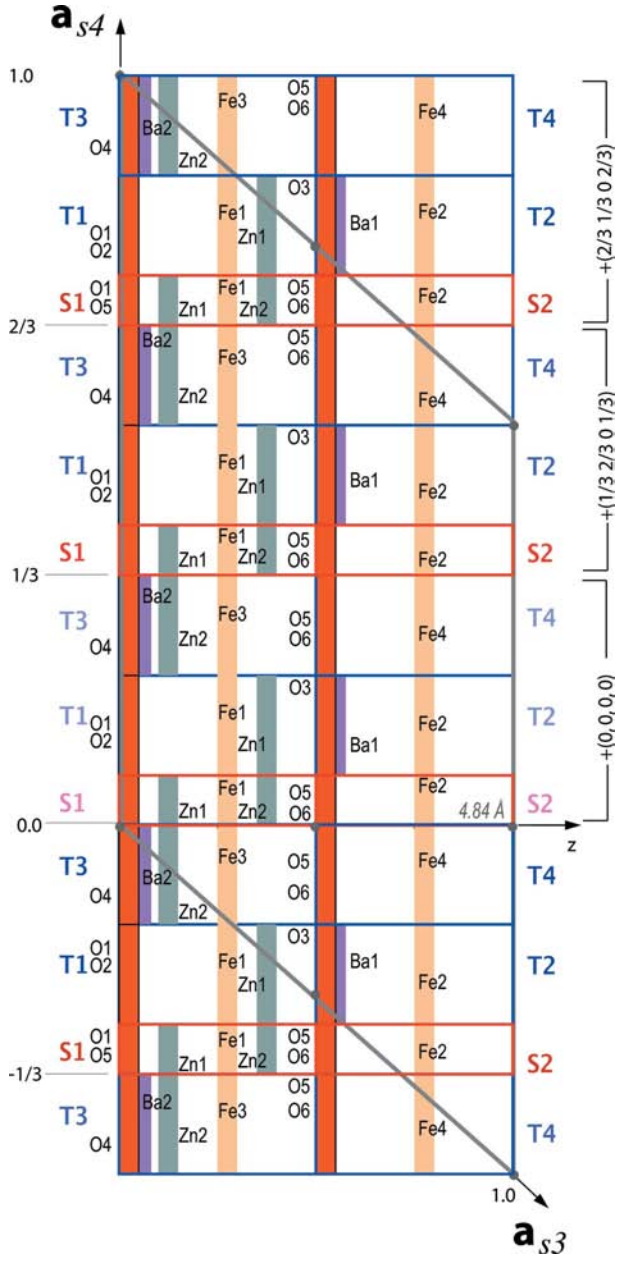

Figure 7
$\mathbf{a}_{s3} - \mathbf{a}_{s4}$ projection of atomic domains of the superspace model. The case $n = 1$ is shown with M = Zn. In this projection the occupation domains for Ba and O atoms coincide. To improve the visibility of the barium domains, they are slightly shifted along z.

[1] As a result, we obtain a superspace construction which can be seen interactively at http://superspace.epfl.ch/ferrites/ (Orlov & Chapuis, 2005). The Flash application allows to change the composition parameter n and move the real-space section with the mouse, thus making it possible to observe the influence of the model parameters on the resulting structure in real time.

[2] An interactive model of the structure with layer resolution can be observed at http://superspace.epfl.ch/ferrites/applet2.html. As in the previous case, it is possible to modify the value of n in the corresponding window and observe the evolution of the layer sequence in real space by dragging the t-line. Note that for convenience the model a_{s3} axes correspond to the nine-times larger c parameter (axes a_{s3}^{applet} in Fig. 6), while the arrangement of the occupation domains remains the same regardless of the cell choice.

Table 4
Basic atomic positions and parameters of the atomic occupation domains for the superspace model of the $(TS)_nT$ series.

* indicates independent atomic positions. The four pairs of atoms marked with the signs ♣, ◇, ♡ and ♠ have connected occupation domains and can be joined into a single occupation domain with the length given by the sum of the lengths of the individual atoms. x_4 center and Δx_4 indicate the position of the center and the width of the occupation domains, respectively.

			Basic position			Occupation domain	
Block	Layer	Atom	x	y	z	x_4 center	Δx_4
T	T1	♣O1_T1*	0	0	0	$\frac{3n+1}{18n+12}$	$\frac{n+1}{9n+6}$
		◇O2_T1*	1/2	0	0		
		Fe1_T1*	2/3	1/3	1/4		
		♡Zn1_T1*	0	0	3/8		
T	T2	Ba1_T2*	1/3	2/3	1/2	$\frac{3n+1}{18n+12}$	$\frac{n+1}{9n+6}$
		O3_T2*	5/6	2/3	1/2		
		Fe2_T2*	2/3	1/3	3/4		
T	T3	O4_T3	1/6	5/6	0	$\frac{5n+3}{18n+12}$	$\frac{n+1}{9n+6}$
		Ba2_T3	2/3	1/3	0		
		Fe3_T3	1/3	2/3	1/4		
		Zn_T3	0	0	1/8		
T	T4	O5_T4	0	0	1/2	$\frac{5n+3}{18n+12}$	$\frac{n+1}{9n+6}$
		O6_T4	0	1/2	1/2		
		♠Fe4_T4*	1/3	1/6	3/4		
S	S1	♣O1_S1*	0	0	0	$\frac{n}{18n+12}$	$\frac{n}{9n+6}$
		◇O5_S1*	1/2	0	0		
		♡Zn1_S1*	2/3	1/3	1/8		
		Fe1_S1*	1/3	2/3	1/4		
		Zn2_S1	0	0	3/8		
S	S2	O5_S2	1/6	5/6	1/2	$\frac{n}{18n+12}$	$\frac{n}{9n+6}$
		O6_S2	2/3	1/3	1/2		
		♠Fe2_S2	1/2	1/2	3/4		

Unfortunately it turned out that detailed structure determinations of the intermediate members of the ferrite family ($0 < n < \infty$) are not available in the literature. The only structure from the TS family available in the ICSD database is the structure of the Y ferrite $Ba_2Zn_2Fe_{12}O_{22}$ ($n = \infty$, $\gamma = \frac{4}{9}$). However, no single-crystal experimental data are available for any of the ICSD entries for this compound.

Therefore, we decided to perform the refinement against a simulated dataset calculated from the published crystal structure. As a starting point we used the structure published by Shin & Kwon (1993). This structure was determined from powder diffraction data; it is the most recent publication and the differences among different published structures are minor. The octahedral positions that are in the ideal ferrite model occupied by a Zn atom are in the published structure partially occupied by Zn and partially by Fe. Since the two atoms have identical parameters, we merged them together and assigned the Zn atomic type to the merged atom. We used this simplified model (which, however, has an identical number of parameters as the real published structure) as a starting point for our calculations.

Using the program *JANA*2000 (Petříček *et al.*, 2000), the amplitudes of the structure factors of the model structure were calculated up to the resolution $\sin\theta/\lambda = 0.7$ Å^{-1}. Then the three-dimensional indices of the calculated reflections were transformed to four-dimensional indexing using $\gamma = \frac{4}{9}$ and a scheme similar to Fig. 5. These reindexed structure factors were then used as 'experimental' data for the refinement of the superspace model. The superspace model was constructed as described in the previous sections. In particular, the $t_0 = \frac{1}{18}$ as follows from Table 2 for the modulation vector $\mathbf{q} = \frac{4}{9}\mathbf{c}^*$, and the origin shift of the space group was set to $(0, 0, -\frac{1}{4}, -\frac{1}{3})$ as

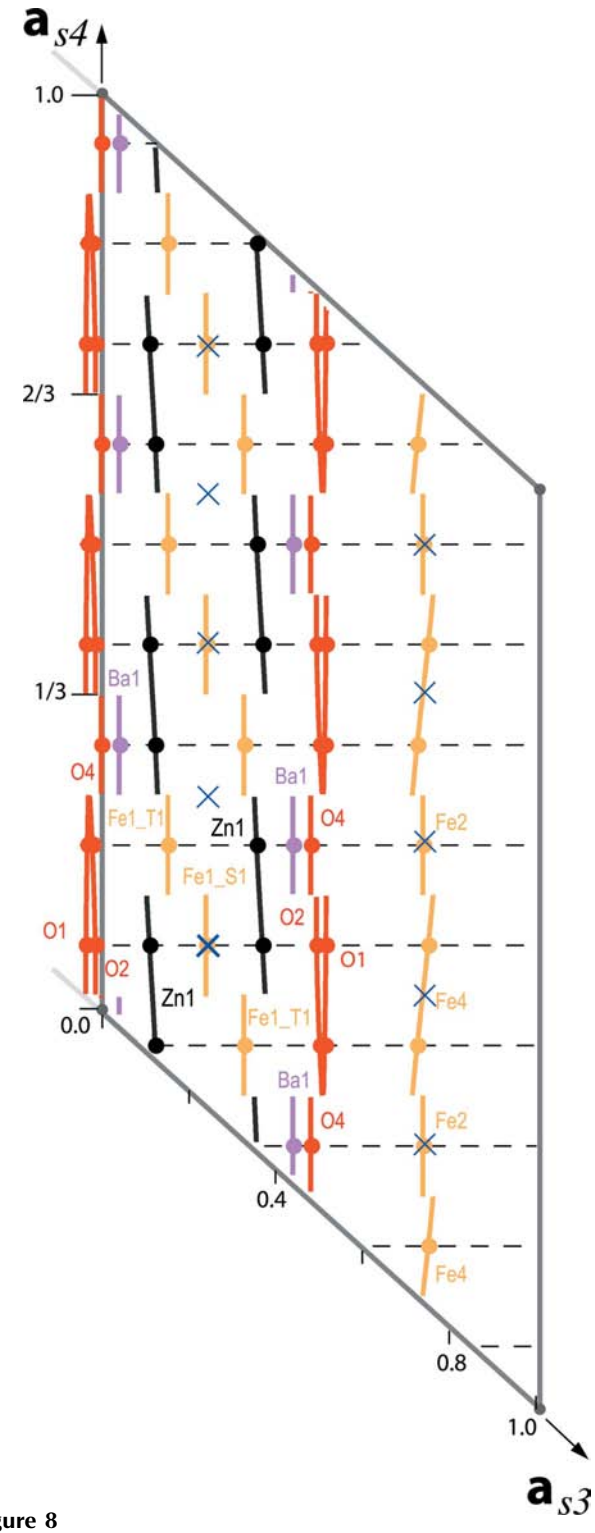

Figure 8
Refined model: $\mathbf{a}_{s3} - \mathbf{a}_{s4}$ projection of atomic domains of the model for the $Ba_2Zn_2Fe_{12}O_{22}$ ($n = \infty$, $t_0 = \frac{1}{18}$) case refined against the simulated data set. The relevant points (three-dimensional atomic positions) are indicated by solid circles, inversion centers by blue crosses. The bold blue cross represents the reference inversion center, used for the calculation of the origin shift of the superspace group (see text for details).

Table 5
The refinement R values of the superspace models refined against a dataset generated from a real structure of Y ferrite.

Model A denotes the full superspace model with all refinable parameters refined. Model B denotes a model with insignificant modulation parameters set to zero.

	Model A	Model B
No. of parameters	47	38
R values R_{all}:		
All reflections	0.0007	0.0052
Main reflections	0.0007	0.0013
First-order sat.	0.0007	0.0027
Second-order sat.	0.0008	0.0060
Third-order sat.	0.0006	0.0077
Fourth-order sat.	0.0005	0.0080

follows from the general formula $\mathbf{s} = (0, 0, -\frac{1}{4}, -\frac{12n+7}{36n+24})$ derived in §6.

The three-dimensional structure of the Y ferrite contains 12 independent atoms. The superspace model contains nine independent atoms (Table 4). The inspection of the models shows that only atoms Zn1_T1, O1_T1 and O2_T1 in the superspace model give rise to two independent atoms in the three-dimensional structure of the Y ferrite. These three atoms thus require a positional modulation to describe the positions of the two independent atoms in the three-dimensional structure. Moreover, the atom Fe4_T4 also requires a positional modulation, because it lies on a special position, but transforms into an atom in the three-dimensional structure that lies on a more general position with two more refinable parameters. In all cases one harmonic wave is sufficient to account for the displacement of the atoms. All other atoms have the same number of refinable parameters in the four-dimensional model as they have in the three-dimensional model, and thus do not require the refinement of an additional displacement modulation. The relationship between the atoms in the four-dimensional model and in the three-dimensional structure is illustrated in Fig. 8.

The three-dimensional model has 47 refinable parameters, and because the four-dimensional model is just an alternative description of the same structure, it must have in the most general case the same number of parameters. When the modulation waves for the position and displacement parameters were added, this condition was indeed fulfilled and the four-dimensional model had 47 refinable parameters. As the generated data were noise-free, the model should fit the data perfectly. This was indeed the case and the refinement R value of all reflections was 0.0007, the remaining tiny difference from zero being most probably due to the different numerical handling of the structures in three-dimensional and four-dimensional models and rounding effects. This refinement confirmed that the four-dimensional model is applicable to real structures and that it offers the same flexibility as the three-dimensional refinement.

The inspection of the refined parameters has shown that all the modulations of the displacement parameters were small and strongly correlated with the average displacement factors. Therefore, these modulation functions were removed from the model. For the same reason the displacement modulation of atom O1_T1 was set to zero. This resulted in a refinement with only 38 refinable parameters (19% less than the full number). Despite the reduction of the number of parameters, the refinement R values increased only slightly ($R_{all} = 0.0052$). The comparison of the refinements is shown in Table 5.

These results confirm the validity of the superspace model and they illustrate how the model can be used to significantly decrease the number of refinable parameters. The reduction of the parameters might seem only moderate in the particularly simple case of the Y ferrite, but might prove crucial in the refinement of the more complex members of the ferrite family.

8. Concluding remarks

We have shown that the ferrites from the $(TS)_nT$ structural family $Ba_{2n+2}M_{2n}Fe_{12n+8}O_{22n+14}$ can all be described as modulated structures with a composition-dependent modulation wavevector. The corresponding superspace model is essentially composition independent and valid for any compound. It is worth stressing that the superspace model is not limited to the case of regular periodic structures, as discussed here, but can also generate aperiodic structures obtained with irrational values of n.

The occupation domains in the idealized superspace model are described by crenel-like functions with a composition-dependent width. The deviations away from the ideal model with rigid layers can be accounted for by means of displacive modulations.

The superspace group of the model is $X\bar{3}m1(00\gamma)$ and the three-dimensional space group for any particular member can be derived by simple rules from this single superspace group. It is the unification of the different symmetries that makes the superspace concept so powerful.

A further important point is that the superspace description allows a significant reduction of the number of refined structural parameters. In the case presented here the number has decreased from the 47 parameters used in the three-dimensional refinement to 38 parameters in the superspace model. It was also shown that the superspace approach is well suited for describing in a unified model the diffraction patterns of simulated structures with different compositions.

The proposed superspace model takes into account the essential structural units of the hexaferrites, which also carry the magnetic properties rigidly associated with them. The presented work makes a first step towards an all-inclusive description of the hexagonal ferrites, in particular embedding the physical properties of ferrites into the superspace.

Supporting information available: the files containing the model of $(TS)_nT$ series in *JANA*2000 format have been deposited.[3]

[3] Supplementary data for this paper are available from the IUCr electronic archives (Reference: SN5054). Services for accessing these data are described at the back of the journal.

The contribution of the Swiss National Science foundation, grant 20-105325/1, is gratefully acknowledged. We also would like to express our thanks to Dr Václav Petříček for his assistance with handling the *JANA*2000 model.

References

Braun, P. B. (1957). *Philips Res. Rep.* **12**, 491–548.
Cornier-Quiquandon, M., Gratias, D. & Katz, A. (1992). *Methods of Structural Analysis of Modulated Structures and Quasicrystals*, edited by J. M. Pérez-Mato, G. Madariaga & F. J. Zúñiga, pp. 313–332. Singapore: World Scientific Publishing Company.
CrystalMaker Software Ltd (2007). *SingleCrystal* 1.3.0 for Mac. CrystalMaker Software Ltd, http://www.crystalmaker.com.
Janssen, T., Chapuis, G. & de Boissieu, M. (2007). *Aperiodic Crystals: From Modulated Phases to Quasicrystals.* Oxford University Press.
Kohn, J. A. & Eckart, D. W. (1963). *J. Phys. Chem.* **67**, 957–958.
Kohn, J. A. & Eckart, D. W. (1965). *J. Appl. Phys.* **36**, 1171–1172.
Kohn, J. A., Eckart, D. W. & Cook, C. F. (1971). *Science*, **172**, 519–525.
Orlov, I. & Chapuis, G. (2004–2007). *Superspace Finder.* Ecole Polytechnique Federale de Lausanne, Switzerland, http://superspace.epfl.ch/finder.
Orlov, I. & Chapuis, G. (2005). *Superspace Interactive Embeddings.* Ecole Polytechnique Federale de Lausanne, Switzerland, http://superspace.epfl.ch.
Pérez-Mato, J. M., Zakhour-Nakhl, M., Weill, F. & Darriet, J. (1999). *J. Mater. Chem.* **9**, 2795–2808.
Petříček, V., Dušek, M. & Palatinus, L. (2000). *JANA*2000. Institute of Physics, Praha, Czech Republic.
Pollert, E. (1985). *Prog. Cryst. Growth Charact. Mater.* **11**, 155–205.
Shin, H.-S. & Kwon, S.-J. (1993). *Powder Diffr.* **8**, 98–101.
Siegrist, T. & Vanderah, T. A. (2003). *Eur. J. Inorg. Chem.* **8**, 1483–1501.
Smaalen, S. van (2007). *Incommensurate Crystallography.* Oxford University Press.
Soohoo, R. (1960). *Theory and Application of Ferrites.* New Jersey: Prentice-Hall.
Tamazyan, R., Arnold, H. & Petříček, V. (1996). *Problems of Modern Crystallography*, pp. 446–466.
Van Landuyt, J., Amelinck, S., Kohn, J. A. & Eckart, D. W. (1973). *Mater. Res. Bull.* **8**, 339–348.
Zakhour-Nakhl, M., Claridge, J. B., Darriet, J., Weill, F., zur Loye, H.-C. & Pérez-Mato, J. M. (2000). *J. Am. Chem. Soc.* **122**, 1618–1623.